# Finite-Set Model Predictive Direct Power Control for DFIG with Reduced Number of Voltage Vectors

Felipe S. Guedes[1], Nady Rocha[2], Alvaro M. Maciel[3], Alfeu J. Sguarezi Filho[4]
[1]Post-Graduate Program in Electrical Engineering (PPGEE), Federal University of Paraíba (UFPB), João Pessoa – PB, Brazil
[2]Electrical Engineering Department (DEE), Federal University of Paraíba (UFPB), João Pessoa – PB, Brazil
[3]Academic Unit III, Electrical Engineering, Federal Institute of Paraíba (IFPB), João Pessoa – PB, Brazil
[4]Center for Engineering, Modeling and Applied Social Sciences (CECS), Federal University of ABC (UFABC), Santo Andre – SP, Brazil
e-mail: felipe.guedes@cear.ufpb.br, nadyrocha@cear.ufpb.br, alvaro.maciel@ifpb.edu.br, alfeu.sguarezi@ufabc.edu.br

***Abstract* – This paper proposes a Simplified Finite-Set Model Predictive Power Controller (MPPC) to improve the performance of the Doubly-Fed Induction Generator (DFIG). The MPPC is implemented to regulate the stator active and reactive powers of DFIG, minimizing the error between them and their references, with an optimized null vector selection and a reduced number of active vectors, to decrease the computational burden. This reduction is applied in a two-level converter, reducing the test to 4 or 2 active vectors. Simulations and laboratory experiments were performed, showing results for a 0.56 kW DFIG. Finally, it was verified that the proposed system can maintain the stator powers at a reference.**

***Keywords* – Direct Power Control (DPC), Doubly-Fed Induction Generator (DFIG), Finite Control Set Model-Based Predictive Control (FCS-MPC), Rotor Side Converter (RSC).**

## I. INTRODUCTION

Doubly-Fed Induction Generator (DFIG) based on wind turbines has some advantages due to the variable speed operation and four-quadrant active/reactive power control capabilities compared with fixed-speed induction generators and synchronous generators [1]. Usually, the DFIG has stator terminals connected directly to the grid, while the rotor is powered by a back-to-back converter. This power converter is employed on the rotor circuit to process the slip power, which is approximately 30% of the rated generator power [2]. A schematic diagram of a DFIG-based wind power generation system is shown in Figure 1.

Ordinarily, DFIGs are controlled by vector control (VC), which decouples the rotor currents into active and reactive components, on either stator-flux-oriented or stator-voltage-oriented [3]. VC can achieve good steady-state performance due to its precise current control. However, the main disadvantage is its linear nature that does not consider the discrete operation of voltage source converters (VSCs) [4]. Furthermore, constraints and nonlinearities of the machine/power converter can not be easily included in the controller design [5].

Manuscript received 06/03/2022; first revision 11/30/2022; accepted for publication 02/23/2023, by recommendation of Editor Telles Brunelli Lazzarin. http://dx.doi.org/10.18618/REP.2023.1.0025

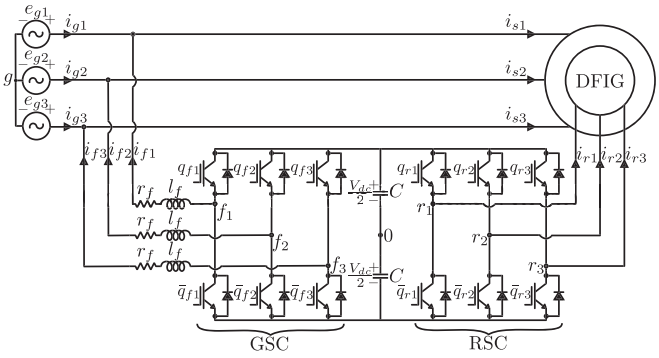


Fig. 1. Schematic of a grid-connected DFIG system.

As an alternative control strategy, the direct power control (DPC) has been proposed for the DFIG [6]. DPC scheme includes a power hysteresis control based on a lookup-table. In general, this control shows the advantages of fast dynamic response and simple structure. However, a large power ripple and a variable switching frequency are obtained.

Model Predictive Control (MPC) is a method that uses the system models to perform an optimization procedure to calculate optimal control actions at each sampling time [7]. The optimization is based on a cost function that minimizes the error between the control variable and its reference. Furthermore, it is possible to add constraints to this function. Since the power converters have a finite number of switching states, the MPC can be simplified and reduced to a Finite Control Set MPC (FCS-MPC) [8].

The FSC-MPC seems to be an efficient method to regulate many applications with static converters. Moreover, FCS-MPC has many characteristics such as fast response, robustness against parameters uncertainty, and external disturbance [9], [10]. This technique is an alternative that was applied in inverters [11]–[14], active power filters [15], [16] and induction machines control [17]–[19]. The predictive functional control and model predictive were applied to DFIG power control by using rotor currents in [20]. The DPC concept was also applied to MPC in [1] and [21], the Model Predictive Power Control, where the control law is derived by optimization of an objective function that considers the control effort and the difference between the predicted active and reactive power, and the specific references.

Several works present predictive control strategies for adverse situations. In [22] proposes a control for unbalanced grid voltages. In [23] simulation results show the FCS-MPC acting in conditions of voltage dip and variable speed. In

[24]–[27] strategies to reduce the power ripple with the multi-vector predictive direct power control, applying more than one vector in a sampling time. In [28] some simplifications to reduce the voltage vectors (VVs) available from a power converter for prediction and actuation, therefore, reducing the computational burden of the MPC, were implemented to a torque control for induction motor drive. In this work, this technique was extended to the MPPC.

This current paper version brings all content of the RSC control previously presented in [37] besides that, new analyses and results are added, among them: optimized zero vector selection; simplifications, and reduction in the numbers of active vectors tested by the control to reduce the computational burden, reducing the test to 4 or 2 active vectors; new simulation and experimental results for a 0.56 kW DFIG. In this way, this paper is organized as follows: the main equations are presented in Section II; the system discretization is presented in Section III; the control strategy structure is presented in Section IV; analysis, simplification, and reductions on active vector are discussed in Section V; simulation and experimental results are presented in Section VI and VII, respectively. Finally, overall conclusions are summarized in Section VIII.

## II. SYSTEM MODELING

Making the $d$ axis synchronous with the grid voltage angle, the $v_{sq}^{v} = 0$ and $v_{sd}^{v} = v_s$, the doubly-fed induction machine model in voltage reference frame is given by [3] as follows

$$\vec{v}_s^{v} = r_s\vec{i}_s^{v} + \frac{d\vec{\lambda}_s^{v}}{dt} + j\omega_v\vec{\lambda}_s^{v} \tag{1}$$

$$\vec{v}_r^{v} = r_r\vec{i}_r^{v} + \frac{d\vec{\lambda}_r^{v}}{dt} + j(\omega_v - P\omega_r)\vec{\lambda}_r^{v} \tag{2}$$

$$\vec{\lambda}_s^{v} = l_s\vec{i}_s^{v} + l_m\vec{i}_r^{v} \tag{3}$$

$$\vec{\lambda}_r^{v} = l_r\vec{i}_r^{v} + l_m\vec{i}_s^{v} \tag{4}$$

$$P_s = v_s^{v} i_{sd}^{v} \tag{5}$$

$$Q_s = -v_s^{v} i_{sq}^{v} \tag{6}$$

$$c_e = 2Pl_m(i_{rd}^{v} i_{sq}^{v} - i_{rq}^{v} i_{sd}^{v}). \tag{7}$$

The subscripts $s$ and $r$ represent the stator and rotor parameters, respectively, $\omega_r$ is the machine speed, $r_s$ and $r_r$ are the stator and rotor resistance, respectively, $l_s$ and $l_r$ are the proper inductances of the stator and rotor windings, respectively, $l_m$ is mutual inductance, $\vec{v}$ is the voltage vector, $\vec{i}$ is the current vector, $\vec{\lambda}$ is the flux vector, $P_s$ and $Q_s$ are the stator active and reactive power, respectively, $v$ index represents the grid-voltage reference frame, $c_e$ is the electromagnetic torque and $P$ is the machine number of pair of poles.

From (1) to (4) the following relationship is found

$$\frac{d\vec{i}_r^{v}}{dt} = \frac{\vec{v}_r^{v} - r_r\vec{i}_r^{v} - \frac{l_m}{l_s}(\vec{v}_s^{v} - r_s\vec{i}_s^{v} - j\omega_r\vec{\lambda}_s^{v}) - j(\omega_v - P\omega_r)\sigma l_r\vec{i}_r^{v}}{\sigma l_r}, \tag{8}$$

where $\sigma$ is the magnetic leakage factor, i.e., $\sigma = 1 - l_m^2/l_s l_r$.

## III. SYSTEM DISCRETIZATION

### A. Rotor Side Converter

The forward Euler method is a well-known first-order numerical procedure for solving ordinary differential equations with a given initial value. Substituting (3), in (5) and (6). After that, applying the differential equation of the rotor current (8), it follows that

$$P_s[k+1] = \frac{v_{sd}^{v}[k+1]}{l_s}\left\{\lambda_{sd}^{v}[k+1] - \frac{l_m T_s}{\sigma l_r}\left[\kappa_d[k] + \omega_{slip}[k]\sigma l_r i_{rq}^{v}[k]\right] - l_m i_{rd}^{v}[k]\right\} \tag{9}$$

$$Q_s[k+1] = \frac{-v_{sd}^{v}[k+1]}{l_s}\left\{\lambda_{sq}^{v}[k+1] - \frac{l_m T_s}{\sigma l_r}\left[\kappa_q[k] - \omega_{slip}[k]\sigma l_r i_{rd}^{v}[k]\right] - l_m i_{rq}^{v}[k]\right\}, \tag{10}$$

where $\omega_{slip} = \omega_v - P\omega_r$, $\vec{\kappa}[k] = \vec{v}_r^{v}[k] - r_r\vec{i}_r^{v}[k] - \frac{l_m}{l_s}\left(\vec{v}_s^{v}[k] - r_s\vec{i}_s^{v}[k] - j\omega_r[k]\vec{\lambda}_s^{v}[k]\right)$, and $T_s$ is the sampling time.

### B. Converter Voltage Representation

The instantaneous converter voltage in the voltage reference frame is obtained with the switching state of the converter and the DC-link voltage. So, the voltage in the Rotor Side Converter (RSC) is

$$v_{rd}^{v}[k] = \sqrt{\frac{2}{3}}V_{dc}[k]\left[cos(\theta_{vr}[k])q_{r1} + cos(\theta_{vr}[k] - \frac{2\pi}{3})q_{r2} + cos(\theta_{vr}[k] + \frac{2\pi}{3})q_{r3}\right] \tag{11}$$

$$v_{rq}^{v}[k] = \sqrt{\frac{2}{3}}V_{dc}[k]\left[-sin(\theta_{vr}[k])q_{r1} - sin(\theta_{vr}[k] - \frac{2\pi}{3})q_{r2} - sin(\theta_{vr}[k] + \frac{2\pi}{3})q_{r3}\right], \tag{12}$$

where $V_{dc}$ is the DC-link voltage, $\theta_{vr} = \theta_v - \theta_r$, $\theta_v$ and $\theta_r$ are the voltage and rotor angles, respectively, and $q_{r123}$ are switching state of the rotor converter.

## IV. PREDICTIVE CONTROL

The control uses measurements of variables into dynamic equations of the system to predict its behavior. Thus, tests are carried out with all possible switching states in the model. The test that obtains the best optimization in the cost function is selected to be applied in the next sampling time. The predictive power control diagram of the RSC is shown in Figure 2. A flowchart of the control algorithm is shown in Figure 3, where $F_{n,RSC}$ is the evaluated cost function when a determined voltage vector $\vec{v_{rn}}$ is applied, where the subindex $n$ means that it is produced by the converter voltage $\vec{v_n}$, with

$n = 0...7$.

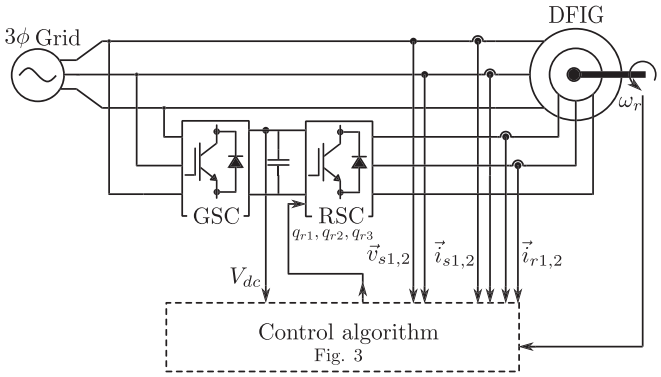


Fig. 2. Predictive power control diagram.

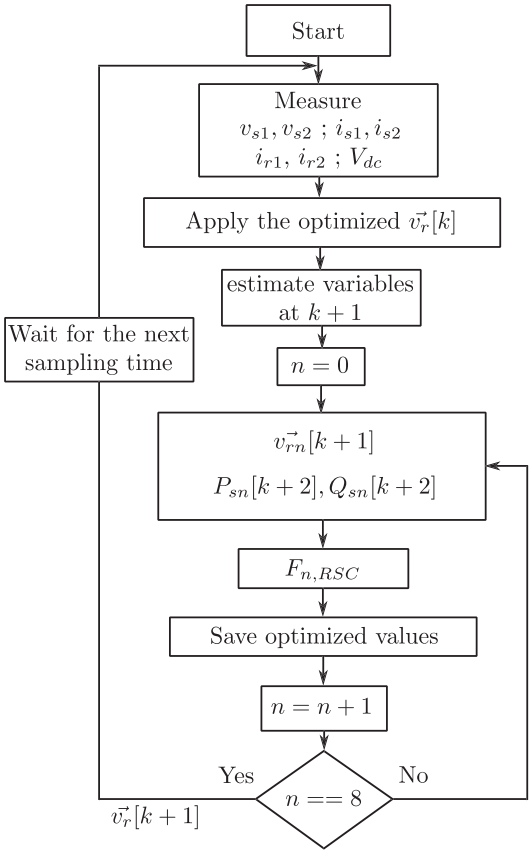


Fig. 3. Flowchart of the implemented control algorithm.

### A. Time-Delay Compensation

To take into account the time delay due to calculations in real-time applications, the algorithm requires two-step-ahead prediction power at $(k+2)th$ instant. The two-step prediction power are calculated using the methodology presented in [30]. Thus, the RSC power, based on equations (9) and (10), can be expressed as

$$P_s[k+2] = \frac{v^v_{sd}[k+2]}{l_s}\left\{\lambda^v_{sq}[k+2] - \frac{l_m T_s}{\sigma l_r}\left[\kappa_d[k+1] + \omega_{slip}[k+1]\sigma l_r i^v_{rq}[k+1]\right] - l_m i^v_{rd}[k+1]\right\} \quad (13)$$

$$Q_s[k+2] = \frac{-v^v_{sd}[k+2]}{l_s}\left\{\lambda^v_{sq}[k+2] - \frac{l_m T_s}{\sigma l_r}\left[\kappa_q[k+1] - \omega_{slip}[k+1]\sigma l_r i^v_{rd}[k+1]\right] - l_m i^v_{rq}[k+1]\right\}. \quad (14)$$

### B. Cost Function

The instantaneous switching state of the RSC generates a rotor voltage vector $\vec{v}_r$ that is applied to the rotor terminals by a two-level voltage source inverter. Only one voltage vector is applied during a sampling time, thus, allows predicting the effect that each voltage vector ($\vec{v_0}...\vec{v_7}$) would have on the stator power.

The active and reactive power control is obtained by the minimization of a cost function $F_n$ for which the inputs are the powers references $P^*_s$ and $Q^*_s$, and the predictions of the powers $P_{sn}[k+2]$ and $Q_{sn}[k+2]$.

$$F_{n,RSC} = \left(P^*_s - P_{sn}[k+2]\right)^2 + \left(Q^*_s - Q_{sn}[k+2]\right)^2. \quad (15)$$

For each rotor voltage vector $\vec{v}_r$ available, this cost function is evaluated, and the rotor voltage producing the minimum cost function is selected to be applied on rotor terminals.

## V. SIMPLIFIED FINITE-SET MODEL PREDICTIVE POWER CONTROL

The structure of the proposed Simplified MPPC (S-MPPC) is almost similar to the conventional MPPC. The differences are the selection of prediction vectors $v_j$ and the cost function design, where $j$ can be three or five values among $j = \{0...7\}$. In the conventional case, all VVs of a 2L-VSI are employed for prediction and actuation. In the proposed S-MPPC, only three – one zero and two active vectors – or five – one zero and four active vectors – of the possible eight VVs are evaluated for prediction and actuation. Therefore, is expected a reduction in the computational burden.

The power prediction on both zero vectors ($v_0$ and $v_7$) produces the same cost value. Thus, only a zero vector ($v_0$) is tested in the predictive control. If this vector generates the lowest cost value, the algorithm select between $v_0$ or $v_7$ in order to minimize the number of switching state changes. Therefore, $v_0$ is selected when the vector in instant $k$ is $v_0$, $v_1$, $v_3$ or $v_5$. Otherwise, $v_7$ is applied.

### A. Simplification for the RSC – 4 active vectors

The proposed control uses the DPC concept proposed in [6]. As shown in [6], the active power depends on angle between rotor and stator flux and reactive power depends on magnitude of rotor flux. From Figure 4, the following conclusions are obtained. Effect of vectors on Active Power: assuming that the rotor flux is located in Sector 1 and counterclockwise rotation, the vectors $\vec{v}_2$ and $\vec{v}_3$ accelerate the rotor flux vector, increasing the angle between the rotor and stator flux by that means there is an increase on the active power. On other hand, the vectors $\vec{v}_5$ and $\vec{v}_6$ decrease angle between them and there is a reduction on the active power.

Effect of vectors on Reactive Power: when the rotor flux vector is localized in sector 1, the vectors $\vec{v}_1$, $\vec{v}_2$ and $\vec{v}_6$ is

responsible to increase the magnitude of rotor flux vector thereby there is a reduction on the stator reactive power and the vectors $\vec{v}_3$, $\vec{v}_4$ and $\vec{v}_5$ is responsible to reduce it, because the rotor flux magnitude is reduced. The impact of active vectors in active and reactive power is summarized in Table I.

Based on a switching Table I, the control has four optimized options to regulate the DFIG power for each rotor flux sector. Hence, knowing the position of the rotor flux in the rotor reference frame, the S-MPPC can use only four active and one zero vectors in the prediction model to evaluate the cost function, reducing the number of the test for each sampling time. The position of the rotor flux in the rotor reference frame ($\theta^r_{\lambda_r}$) is estimated as

$$\theta^r_{\lambda_r} = tan^{-1}(\lambda^s_{rq}/\lambda^s_{rd}) - \theta_r, \tag{16}$$

where $\lambda_r$ is the rotor flux, superscript $s$ represents the stationary reference frame and $\theta_r$ is the rotor position.

The active VVs change periodically by an angle $\pi/3$ rad steps, as shown in Figure 4. Accordingly, the $d-q$ plane in stationary reference frame is divided into six sectors to identify the direction of rotation as

$$(2N_{rsc}-3)\pi/6 \leq \theta_{N_{rsc}} \leq (2N_{rsc}-1)\pi/6, \tag{17}$$

where $\theta_{N_{rsc}}$ is the sector and $N_{rsc} = 1, ..., 6$.

In order to choose the active vectors, the present sector of the rotor flux has to be identified. The voltage vectors that will be tested correspond to four active vectors shown in Table I of the corresponding sector plus a zero vector. As an example, if the rotor flux vector is in Sector 1, the tested voltage vectors are $\vec{v}_3$, $\vec{v}_2$, $\vec{v}_5$, $\vec{v}_6$ and $\vec{v}_0$.

In this method, it is possible to reduce the test in two vectors. However, this control requires the estimates of the rotor flux and its sector, increasing the computational burden.

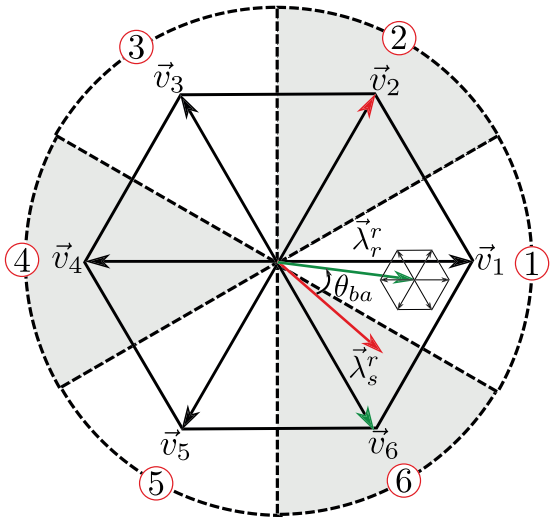


Fig. 4. Six-sector division method in the $d-q$ plane.

*B. Simplification for the RSC – 2 active vectors*

For a greater simplification in the number of vectors that will be tested, one of the power magnitudes can already have its change predetermined. Therefore, there are two options to simplify the vectors:

1. previously check the active power error conditions, $P_{s,e}$ in Table I; or
2. check the error in reactive power conditions, $Q_{s,e}$ in Table I.

**TABLE I**
**Optimized Switching Table for DPC-DFIG**

| Conditions | | Sector $\vec{\lambda}^r_r$ | | | | | |
|---|---|---|---|---|---|---|---|
| | | 1 | 2 | 3 | 4 | 5 | 6 |
| $P_{s,e} \leq 0$ | $Q_{s,e} > 0$ | $\vec{v}_3$ | $\vec{v}_4$ | $\vec{v}_5$ | $\vec{v}_6$ | $\vec{v}_1$ | $\vec{v}_2$ |
| | $Q_{s,e} \leq 0$ | $\vec{v}_2$ | $\vec{v}_3$ | $\vec{v}_4$ | $\vec{v}_5$ | $\vec{v}_6$ | $\vec{v}_1$ |
| $P_{s,e} > 0$ | $Q_{s,e} > 0$ | $\vec{v}_5$ | $\vec{v}_6$ | $\vec{v}_1$ | $\vec{v}_2$ | $\vec{v}_3$ | $\vec{v}_4$ |
| | $Q_{s,e} \leq 0$ | $\vec{v}_6$ | $\vec{v}_1$ | $\vec{v}_2$ | $\vec{v}_3$ | $\vec{v}_4$ | $\vec{v}_5$ |

In each scenario, and with a certain error of the selected power, only two lines from Table I can be used.

The control checks whether this selected power needs to increase or decrease. With this predetermined direction, the control manages to reduce the number of vectors that will be tested in the model, restricting only the two active vectors that cause different impacts on the power that was not pre-selected and the null vector.

For a better understanding, an example can be used. In this example, the selected power is $Q_s$. In this way, from the measurement and reference of this quantity, the error is obtained. So, to reduce this error, which can be $Q_{s,e} \leq 0$ or $Q_{s,e} > 0$, the Table I offers only two active vectors as a solution, which change according to the sector of the rotor flux. So, only these two active vectors and one null vector are tested in predictive control. Therefore, if $Q_{s,e} \leq 0$ and the rotor flux is in sector 1, only the vectors $\vec{v}_0$, $\vec{v}_2$ and $\vec{v}_6$ will be tested in the model by the control, and the vector selected is that one, among the three, which best minimize the cost function. If $Q_{s,e} > 0$ and the rotor flux is the same, the selected vectors would be $\vec{v}_0$, $\vec{v}_3$ and $\vec{v}_5$.

## VI. SIMULATION RESULTS

The overall proposed control scheme for a DFIG-based on wind generation has been tested through simulation using the software PSIM® 2020a. The simulation parameters are shown in Table II. The DC-link voltage is 311 V, the sampling time ($T_s$) is 100 $\mu$s and grid voltage ($v_s$) is 127 V (RMS).

**TABLE II**
**Machine Parameters**

| Parameter | Value | Parameter | Value |
|---|---|---|---|
| $P_n$ | 560 (W) | $l_s$ | 563.7 (mH) |
| $V_n$ | 220 (V) | $l_r$ | 543.7 (mH) |
| $r_s$ | 15.1 ($\Omega$) | $l_m$ | 523.8 (mH) |
| $r_r$ | 6.22 ($\Omega$) | J | 0.013 (Kg/m$^2$) |
| $V_r$ | 200 V (RMS) | | |

Four cases will be analyzed where the RSC controls are tested in the same simplification scenario.

- Case 1: Conventional control;
- Case 2: Four active vectors;
- Case 3: Two active vectors $P_{s,e}$;
- Case 4: Two active vectors $Q_{s,e}$.

Initially, the stator active and reactive power references were 0, and then, the active power reference was set to -500W at t = 1.5s. The reactive power reference was maintained at 0

**TABLE III**
**RSC comparison result**

| Cases | $\bar{P}_s$ [W] | $\bar{Q}_s$ [var] | SSE | $f_s$ [Hz] | Rising Time | Settling Time | THD $i_s$ |
|---|---|---|---|---|---|---|---|
| 1 | -498,60 | 0,02 | 0,54 | 2028,5 | 1.11 ms | 0.133 s | 3.23% |
| 2 | -497,85 | 3,37 | 0,80 | 2031,0 | 1.06 ms | 0.160 s | 3.29% |
| 3 | -496,55 | 6,47 | 1,47 | 1897,7 | 1.06 ms | 0.171 s | 3.36% |
| 4 | -495,65 | 4,49 | 1,25 | 2048,5 | 1.05 ms | 0.167 s | 3.28% |

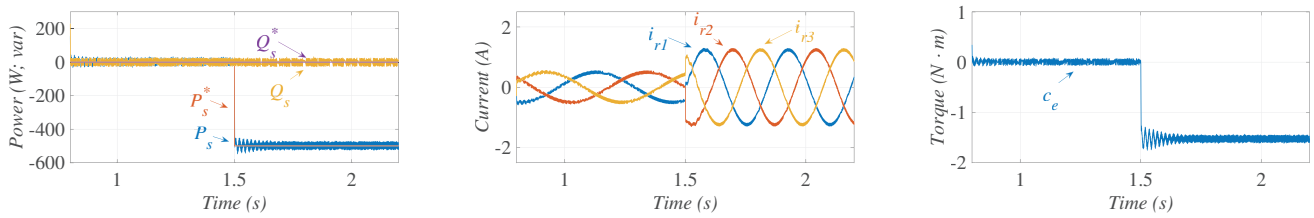


(a) (b) (c)

Fig. 5. Conventional FS-MPPC simulation results: (a) Stator active $(P_s)$ and reactive $(Q_s)$ power. (b) Rotor currents $(i_{r1}, i_{r2}$ and $i_{r3})$. (c) Electromagnetic torque $(c_e)$.

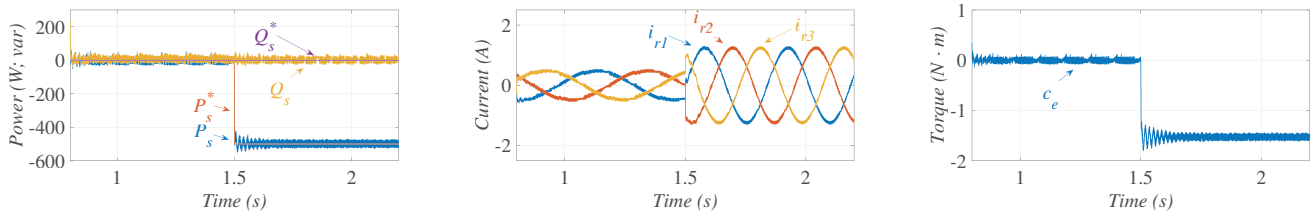


(a) (b) (c)

Fig. 6. Four vectors S-MPPC simulation results: (a) Stator active $(P_s)$ and reactive $(Q_s)$ power. (b) Rotor currents $(i_{r1}, i_{r2}$ and $i_{r3})$. (c) Electromagnetic torque $(c_e)$.

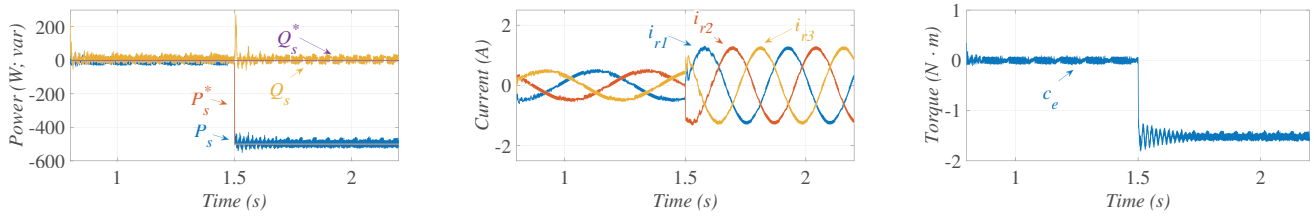


(a) (b) (c)

Fig. 7. Two vectors $P_s$ pre-selected S-MPPC simulation results: (a) Stator active $(P_s)$ and reactive $(Q_s)$ power. (b) Rotor currents $(i_{r1}, i_{r2}$ and $i_{r3})$. (c) Electromagnetic torque $(c_e)$.

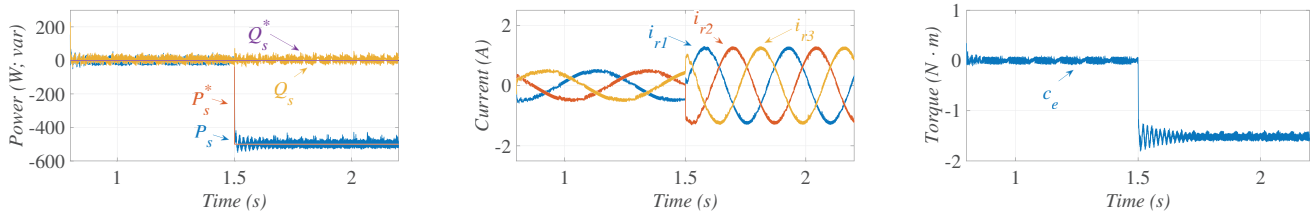


(a) (b) (c)

Fig. 8. Two vectors $Q_s$ pre-selected S-MPPC simulation results: (a) Stator active $(P_s)$ and reactive $(Q_s)$ power. (b) Rotor currents $(i_{r1}, i_{r2}$ and $i_{r3})$. (c) Electromagnetic torque $(c_e)$.

var. The grid-side converter control is based on [29] and [37]. The speed and rotor position estimations is based on [31].

Figures 5 to 8 show the simulation results for the four cases on the RSC. Comparative results between the methods

are shown in Table III. Generating these results, the metrics and concepts seen in [36] are used. This table presents, respectively, the average of steady-state powers, the Steady-State Error (SSE), the average frequency of switching ($f_s$) in steady-state, the Rising Time, and the Settling time. The results in steady-state were obtained with active power equal to 500 W, while the rising time and the settling time were obtained considering a step from 0 to 500W (generator nominal value) in active power.

In general, the results in the steady-state are similar, with small deviations in the averages of the powers to their reference. Case 4 obtained the worst scenario in the active power, -495.65 W, and Case 3, in the reactive power with 6.47 var. It is observed an increase in the standard deviation of the power with the reduction of vectors, in other words, with the reduction of the number of vectors, the power values are further from the mean, also presenting occasional spikes.

The average harmonic distortions of the stator currents around 60 Hz are close, being case 3 the worst case with 3.36%. Case 1, with 3.23%, is the best THD scenario.

The switching frequency remained close, except in Case 3, where the reduction is almost 10% compared to case 1, this justifies the small increase in THD in case 3 when compared to case 1.

As for the rise time, which is the time it takes for the system to reach 90% of the reference during a transient, the cases with vector reduction presented a better performance, obtaining 1.06 ms. Finally, the accommodation time, the time it takes for the variable to reach the threshold of $\pm 25$ [W, var], of case 1 was lower than the others, with 0.133 s.

Cases 2, 3, and 4 also exhibit good dynamic performance, with a maximum of 0.17 s of settling-time, during the change of the active power. However, the active vectors in case 3, shown in Figure 7, were not enough in the transitional causing an unwanted spike in reactive power. Moreover, case 4 presents some spikes in the powers that can be observed mainly in the active power, reaching -450 W, illustrated in Figure 8.a, increasing the standard deviation.

In all scenarios, the ripple of the active and reactive powers are $\pm$ 25 W, the electromagnetic torque shows no permanent oscillations, and the rotor currents in the stationary reference frame increase from 0.55 A to 1.29 A, as the active power injected into the grid increases.

Cases 1, 2, and 4 show similar simulation results. Case 4, therefore, becomes a viable option since the computational cost is the lowest among these three cases, due to the use of only two active vectors.

The FS-MPPC and S-MPPC performances in other active power scenarios are illustrated in Figure 9. Initially, the stator active and reactive power references were 0, and then, the active power reference was set to:

- -200W at t = 1.5s to t = 2s;
- -500W at t = 2s to t = 2.5s;
- -100W at t = 2.5s to t = 3s.

It can be seen that the control system works properly, despite the reduction in the number of active vectors tested in each sampling time.

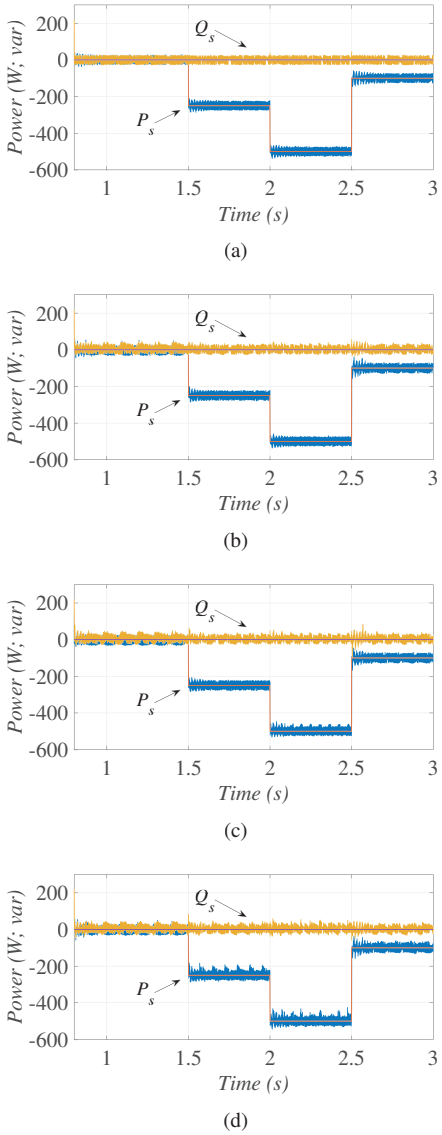


Fig. 9. The MPPC simulation results in others Stator active power ($P_s$) reference values. (a) Conventional FS-MPPC. (b) Four vectors S-MPPC. (c) Two vectors $P_s$ pre-selected S-MPPC. (d) Two vectors $Q_s$ pre-selected S-MPPC.

## VII. EXPERIMENTAL RESULTS

### *A. Experimental Setup*

In order to validate the FCS-MPC, the system was implemented in laboratory. In this scheme, the stator of the machine is connected direct to a 220 V three-phase electrical grid and the rotor voltages are being fed by the RSC. The DC-link voltage was adjusted to 311 V, and was fed by a full-bridge rectifier connected to the three-phase grid instead of using the GSC, in order to simplify the experiment. As long the DFIG operates in synchronous or subsynchronous modes, as the rotor circuit does not provide power to the system, the unidirectional rectifier is sufficient to perform the tests. The experimental was based on a digital signal processor (DSP), model TMS320F28335, with a microcomputer equipped with appropriate plug-in boards and sensors. The converter use power switches model SKM50GB123D. Since the system is three-phase balanced, the values of $i_{s3}$, $i_{r3}$ and $v_{s3}$ were

estimated from the measured values $i_{s12}$, $i_{r12}$ and $v_{s12}$. The results were obtained by a Agilent oscilloscope, model DSO-X 3014A. The sampling time $T_s$ was 1/15000 s.

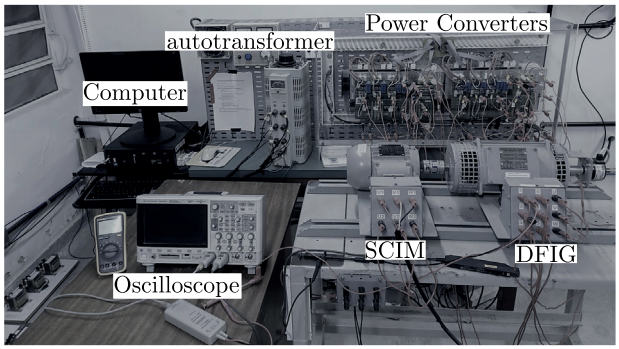


Fig. 10. Experimental setup, system overview.

The machines used in the experiment are shown in Figure 10. The mechanical torque was provided by a 0.55 kW (220 V, 60 Hz) Squirrel Cage Induction Machine (SCIM), electrically fed directly by an autotransformer. The system is direct coupled to a 0.56 kW DFIG. Other DFIG parameters are listed in Table II. A power observer based on [38], was used to improves the robustness of the system.

*B. Results*

Figure 11 illustrates the powers in a steady-state. The reactive power reference is zero ($Q_s^*$ =0) and active power reference is -500 W ($P_s^*$ = -500 W). In this figure, the instantaneous values of power show a larger ripple and some eventual spikes compared to the simulation. The average power values are also indicated, being in the conventional case -16.9 var for the reactive power and -496.3 W for the active. Note that the powers oscillate over the reference.

Figure 12 shows the result of the torque with their respective average values. Case 3 has less ripple and a mean of -1.27 Nm. Case 4 also had a good result, but with some spikes that reach up to -2.5 Nm. The average value of the latter was -1.32 Nm. The speed averages are similar, not exceeding a 2% difference, and case 1 was from 342.1 rad/s.

The stator voltage and current are illustrated in Figure 13. The voltages are close to 127 V (RMS). As for the stator currents, the RMS values are approximately 1.25 A. The stator currents values are lagged 180° from the stator voltages, indicating that the system is generating power at unit power factor.

The rotor currents are illustrated in Figure 14. The RMS values are approximately 1.2 *A*. It can be noted that the rotor currents frequencies are very low (6 Hz approximately), indicating that the system is operating near the synchronous speed.

Table IV shows the average values of active and reactive powers and the percentage of control processing time by the DSP within a sampling cycle. Thus, the value of 60.52% of case 1 indicates that this control takes 40.34 $\mu$s to be executed, as the sampling time is 66.67 $\mu$s. It is observed that Case 2, despite the reduction of the number of vectors tested for sampling time, increases the processing by 2.2%, compared to Case 1, due to the addition of the rotor flux estimator to identify the sector. On the other hand, Cases 3 and 4, reduce the computational burden by 6.3% and 6.1%, respectively, and preserve a similar performance to the conventional MPPC.

**TABLE IV**
**Experimental results of vector reduction in RSC control**

| Cases | $\bar{P}_s$ [W] | $\bar{Q}_s$ [var] | Computational burden |
|---|---|---|---|
| 1 | -496,3 | -16,9 | 60,52% |
| 2 | -504,1 | -11,2 | 61,87% |
| 3 | -491,2 | -6,1 | 56,70% |
| 4 | -499,8 | -7,9 | 56,85% |

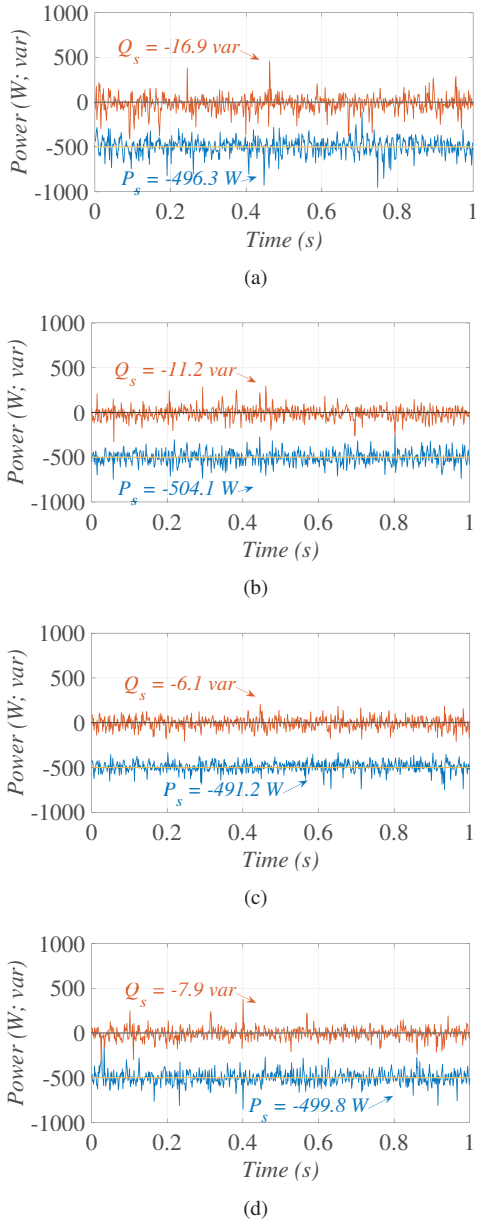


Fig. 11. Experimental results: stator active $(P_s)$ and Reactive $(Q_s)$ power. (a) Case 1. (b) Case 2. (c) Case 3. (d) Case 4.

## VIII. CONCLUSIONS

This paper presents a simplified finite-set model predictive power control applied to the RSC for a DFIG. The control law is designed to generate the switching state of the RSC

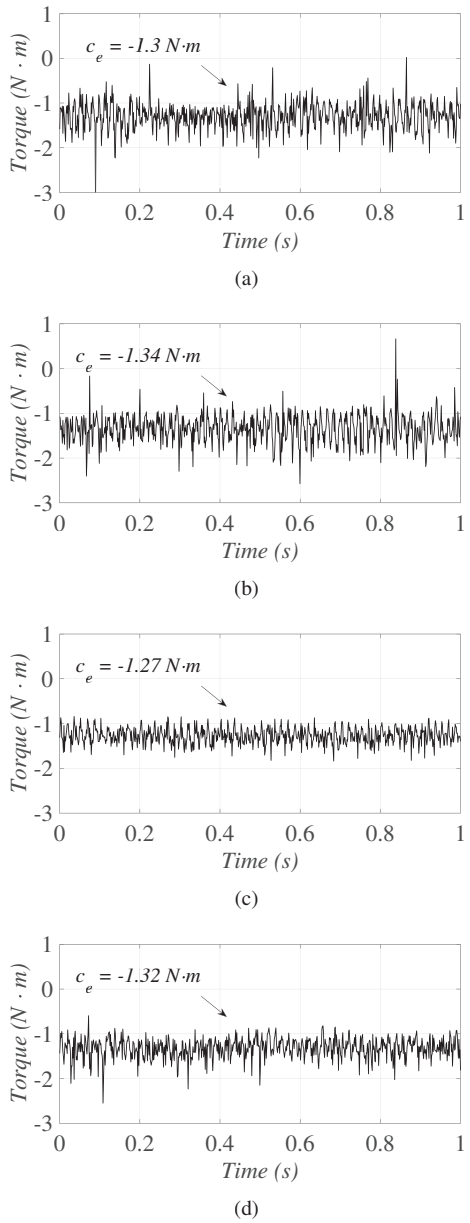


Fig. 12. Experimental results: electromagnetic torque $(c_e)$. (a) Case 1. (b) Case 2. (c) Case 3. (d) Case 4.

based on the active and reactive power errors. Simulation and experimental results confirm the effectiveness of the system, presenting performance comparisons of controls with a reduced number of active vectors. Considering the Cases 3 and 4, simulation results show the Steady-State Error (SSEs) for active power are greater than the case 1, however they are below the 1.5 %. In addition, the control exhibits fast dynamics despite the smaller number of active vectors. Experimental steady-state results show that the S-MPPC can maintain the DFIG at a power reference, and generate power at unit power factor. From these results, the S-MPPC has a similar performance than the conventional MPPC. If the computational burden is the metric, Case 3 is the best choice, with a reduction of 6.31% in the computational burden compared with the conventional MPPC. However, Case 4 has a better dynamic response and smaller steady-state than Case 3, being an interesting choice.

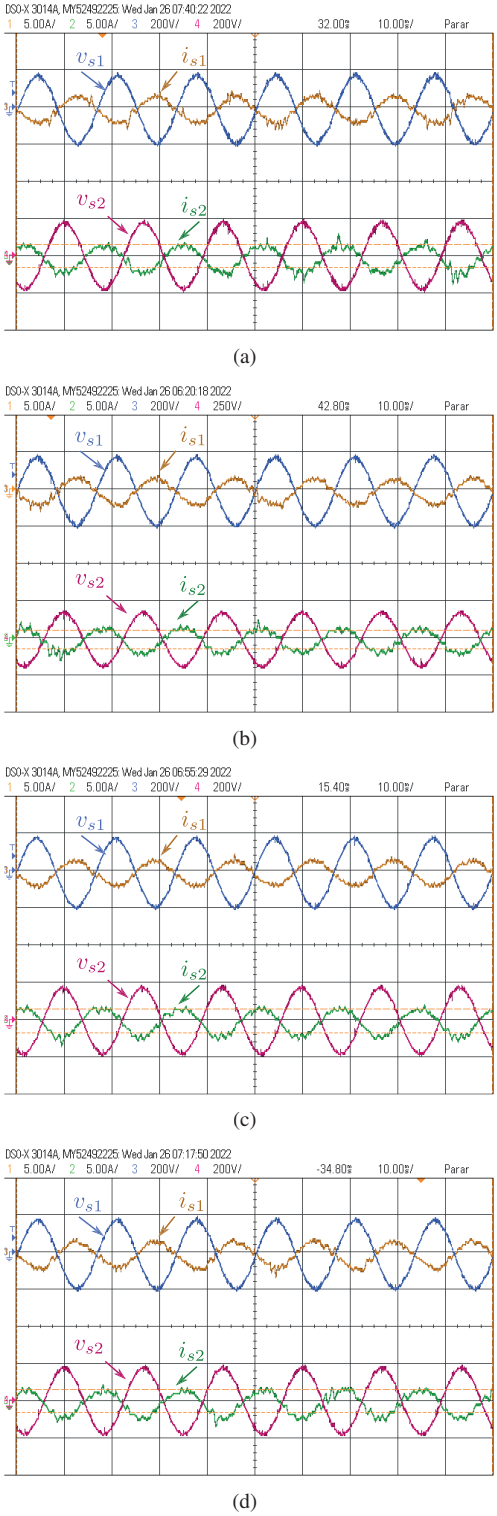


Fig. 13. Experimental results: stator voltages $(v_{s1}$ and $v_{s2})$ and currents $(i_{s1}$ and $i_{s2})$. Time (10 ms/div). Voltage (200V/div). Current (5A/div). (a) Case 1. (b) Case 2. (c) Case 3. (d) Case 4.

## ACKNOWLEDGEMENTS

This work was supported in part by the Coordenação de Aperfeiçoamento de Pessoal de Nível Superior – Brasil (CAPES) – Finance Code 001 and in part by the Conselho Nacional de Desenvolvimento Científico e Tecnológico CNPq.

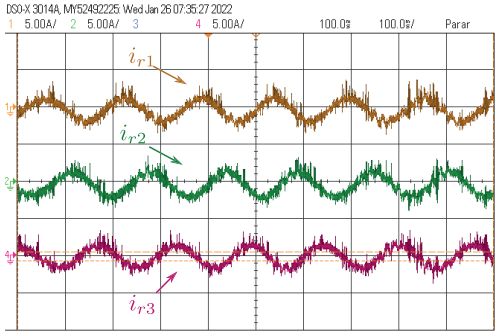


(a)

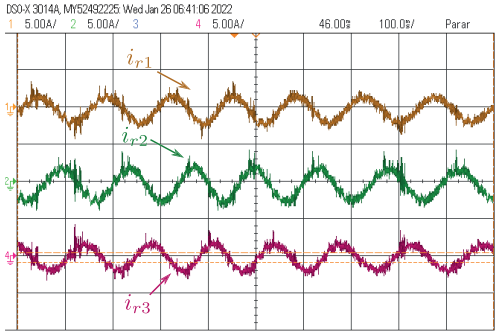


(b)

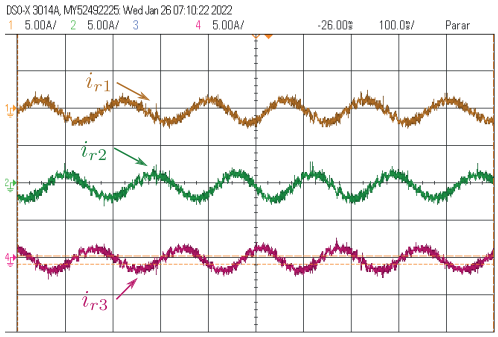


(c)

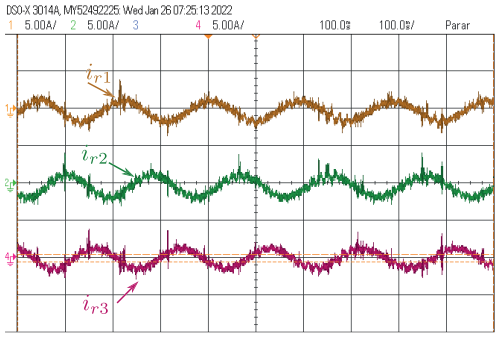


(d)

Fig. 14. Experimental results: rotor currents ($i_{r1}$, $i_{r2}$ and $i_{r3}$). Time (100 ms/div). Current (5A/div). (a) Case 1. (b) Case 2. (c) Case 3. (d) Case 4.

## REFERENCES


[1] A. J. Sguarezi Filho, E. R. Filho, "Model-Based Predictive Control Applied to the Doubly-Fed Induction Generator Direct Power Control," *IEEE Transactions on Sustainable Energy*, vol. 3, no. 3, pp. 398–406, Jul. 2012.

[2] V. Yaramasu, B. Wu, P. C. Sen, S. Kouro, M. Narimani, "High-power wind energy conversion systems: State-of-the-art and emerging technologies," *Proceedings of the IEEE*, vol. 103, no. 5, pp. 740–788, 2015.

[3] S. Muller, M. Deicke, R. W. De Doncker, "Doubly fed induction generator systems for wind turbines," *IEEE Industry Applications Magazine*, vol. 8, no. 3, pp. 26–33, May–Jun. 2002.

[4] M. Abdelrahem, R. Kennel, "Efficient Direct Model Predictive Control for Doubly-Fed Induction Generators," *Electric Power Components and Systems*, vol. 45, no. 5, pp. 574–587, Mar. 2017.

[5] M. Abdelrahem, C. Hackl, J. Rodríguez, R. Kennel, "Improved Direct-Model Predictive Control with a Simple Disturbance Observer for DFIGs," *in 22nd European Conference on Power Electronics and Applications (EPE '20 ECCE Europe)*, pp. P.1–P.9, 2020.

[6] R. Datta, V. T. Ranganathan, "Direct power control of grid-connected wound rotor induction machine without rotor position sensors," *IEEE Transactions on Power Electronics*, vol. 16, no. 3, pp. 390–399, May 2001.

[7] J. Rodriguez, J. Pontt, C. A. Silva, P. Correa, P. Lezana, P. Cortes, U. Ammann, "Predictive Current Control of a Voltage Source Inverter," *IEEE Transactions on Industrial Electronics*, vol. 54, no. 1, pp. 495–503, Feb. 2007.

[8] S. Kouro, P. Cortes, R. Vargas, U. Ammann, J. Rodríguez, "Model Predictive Control – A Simple and Powerful Method to Control Power Converters," *IEEE Transactions on Industrial Electronics*, vol. 56, no. 6, pp. 1826–1838, Jun. 2009.

[9] A. A. Z. Diab, "Model Predictive Direct Power Control of Rotor Side Converter for DFIGs Driven by Variable Speed Wind Turbines," *in 25th International Workshop on Electric Drives: Optimization in Control of Electric Drives (IWED)*, pp. 1–6, 2018.

[10] S. V. Dias, T. R. F. Neto, L. L. N. Reis, B. C. Torrico and J. C. T. Campos, "Controlador de Corrente Preditivo Contínuo com Anti-Windup Aplicado a um Sistema de Geração Eólico Baseado em DFIG," *Brazilian J. Power Electron. – SOBRAEP*, vol. 22, no. 1, pp. 71–80, Jan. 2017. doi: 10.18618/REP.2017.1.2650.

[11] F. Herrera, R. Cárdenas, M. Rivera, J. A. Riveros and P. Wheeler, "Predictive Voltage Control Operating at Fixed Switching Frequency of a Neutral-Point Clamped Converter," *in IEEE 15th Brazilian Power Electronics Conference and 5th IEEE Southern Power Electronics Conference (COBEP/SPEC)*, pp. 1–6, 2019. doi: 10.1109/COBEP/SPEC44138.2019.9065819.

[12] P. C. de S. Furtado and P. Gomes Barbosa, "Model Predictive Controller for Two-Phase Three-Wire Grid-Connected Converters," *in IEEE 15th Brazilian Power Electronics Conference and 5th IEEE Southern Power Electronics Conference (COBEP/SPEC)*, pp. 1–6, 2019. doi: 10.1109/COBEP/SPEC44138.2019.9065666.

[13] S. Yan, Y. Yang, S. Y. Hui and F. Blaabjerg, "A Review on Direct Power Control of Pulsewidth Modulation Converters," *IEEE Transactions on Power Electronics*, vol. 36, no. 10, pp. 11984–12007, Oct. 2021. doi: 10.1109/TPEL.2021.3070548.

[14] C. Garcia et al., "FCS-MPC Based Pre-Filtering Stage for Computational Efficiency in a Flying Capacitor Converter," *IEEE Access*, vol. 9, pp. 111039–111049, Aug. 2021. doi: 10.1109/ACCESS.2021.3103070.

[15] P. Zanchetta, P. Cortes, M. Perez, J. Rodriguez, C. Silva, "Finite States Model Predictive Control for Shunt Active Filters," *in 37th Annual Conference of the IEEE Industrial Electronics Society (IECON)*, pp. 581–586, 2011.

[16] J. G. L. Foster, R. R. Pereira, R. B. Gonzatti, W. C. Sant'Ana, D. Mollica and G. Lambert-Torres, "A Review of FCS-MPC in Multilevel Converters Applied to Active Power Filters," *in IEEE 15th Brazilian Power Electronics Conference and 5th IEEE Southern Power Electronics Conference (COBEP/SPEC)*, pp. 1–6, 2019. doi: 10.1109/COBEP/SPEC44138.2019.9065398.

[17] H. Miranda, P. Cortes, J. I. Yuz, J. Rodriguez, "Predictive Torque Control of Induction Machines Based on State-Space Models," *IEEE Transactions on Industrial Electronics*, vol. 56, no. 6, pp. 1916–1924, Jun. 2009.

[18] A. F. B. Filho, F. E. C. Souza, L. P. S. Júnior, J. S. B. Lopes, A. O. Salazar and W. L. A. Silva, "Uma avaliação de métodos de controle preditivo aplicados a um motor de indução," *Brazilian J. Power Electron. – SOBRAEP*, vol. 22, no. 2, pp. 187–195, Apr. 2017. doi: 10.18618/REP.2017.2.2672.

[19] A. S. Lunardi and A. J. Sguarezi Filho, "Controle preditivo baseado em modelo para sistema eólico empregando gerador de indução gaiola de esquilo," *Brazilian J. Power Electron. – SOBRAEP*, vol. 23, no. 3, pp. 330–338, Jul. 2018. doi: 10.18618/REP.2018.3.2788.

[20] M. Abdelrahem, R. Kennel, C. M. Hackl, J. Rodríguez, "Simple and Robust Finite-Control-Set Model Predictive Control for DFIGs in Wind Turbine Systems," *in 2020 11th Power Electronics, Drive Systems, and Technologies Conference (PEDSTC)*, pp. 1–6, 2020.

[21] Y. Zhang, J. Jiao, D. Xu, D. Jiang, Z. Wang, C. Tong, "Model Predictive Direct Power Control of Doubly Fed Induction Generators Under Balanced and Unbalanced Network Conditions", *IEEE Transactions on Industry Applications*, vol. 56, no. 1, pp. 771–786, Feb. 2020.

[22] J. Hu, J. Zhu and D. G. Dorrell, "Predictive Direct Power Control of Doubly Fed Induction Generators Under Unbalanced Grid Voltage Conditions for Power Quality Improvement," *IEEE Transactions on Sustainable Energy*, vol. 6, no. 3, pp. 943–950, Jul. 2015.

[23] S. Saeidi, R. A. de Marchi and E. Bim, "Nonlinear predictive control for a DFIG under voltage dip," *in 42nd Annual Conference of the IEEE Industrial Electronics Society (IECON)*, pp. 1955–1960, 2016.

[24] A. M. Bozorgi, H. Gholami-Khesht, M. Farasat, S. Mehraeen and M. Monfared, "Model Predictive Direct Power Control of Three-Phase Grid-Connected Converters With Fuzzy-Based Duty Cycle Modulation," *IEEE Transactions on Industry Applications*, vol. 54, no. 5, pp. 4875–4885, Sept.–Oct. 2018. doi: 10.1109/TIA.2018.2839660.

[25] D. Zhou, P. Tu and Y. Tang, "Multivector Model Predictive Power Control of Three-Phase Rectifiers With Reduced Power Ripples Under Nonideal Grid Conditions," *IEEE Transactions on Industrial Electronics*, vol. 65, no. 9, pp. 6850–6859, Sep. 2018. doi: 10.1109/TIE.2018.2798583.

[26] S. Yan, J. Chen, T. Yang and S. Y. Hui, "Improving the Performance of Direct Power Control Using Duty Cycle Optimization," *IEEE Transactions on Power Electronics*, vol. 34, no. 9, pp. 9213–9223, Sep. 2019. doi: 10.1109/TPEL.2018.2883425.

[27] S. Yan and S. Y. R. Hui, "A Simple Multi-Vector Predictive Direct Power Control Using Geometric Modulation," *IEEE Transactions on Power Electronics*, vol. 37, no. 3, pp. 2899–2908, Mar. 2022. doi: 10.1109/TPEL.2021.3118702.

[28] M. Habibullah, D. D. Lu, D. Xiao and M. F. Rahman, "A Simplified Finite-State Predictive Direct Torque Control for Induction Motor Drive," *IEEE Transactions on Industrial Electronics*, vol. 63, no. 6, pp. 3964–3975, Jun. 2016.

[29] L. Tarisciotti, A. Formentini, A. Gaeta, M. Degano, P. Zanchetta, R. Rabbeni, M. Pucci, "Model Predictive Control for Shunt Active Filters With Fixed Switching Frequency," *IEEE Transactions on Industry Applications*, vol. 53, no. 1, pp. 296–304, Jan.–Feb. 2017.

[30] P. Cortés, J. Rodríguez, D. Quevedo, and C. Silva, "Predictive current control strategy with imposed current spectrum," *IEEE Trans. Power Electron.*, vol. 23, no. 2, pp. 612–618, Mar. 2008.

[31] E. L. Soares, F. V. Rocha, L. M. S. de Siqueira and N. Rocha, "Sensorless Rotor Position Detection of Doubly-Fed Induction Generators for Wind Energy Applications," *in 13th IEEE International Conference on Industry Applications (INDUSCON)*, pp. 1045–1050, 2018. doi: 10.1109/INDUSCON.2018.8627227.

[32] B. S. Chen and G. Joós, "Direct Power Control of Active Filters With Averaged Switching Frequency Regulation," *IEEE Transactions on Power Electronics*, vol. 23, no. 6, pp. 2729–2737, Nov. 2008. doi: 10.1109/TPEL.2008.2004958.

[33] H. Afghoul and F. Krim, "Comparison between PI and fuzzy DPC control of a shunt active power filter," *in IEEE International Energy Conference and Exhibition (ENERGYCON)*, pp. 146–151, 2012. doi: 10.1109/EnergyCon.2012.6347742.

[34] H. Afghoul, F. Krim, D. Chikouche, A. Beddar and B. Babes, "Implementation of Direct Power Control

for shunt active power filter," *in 3rd International Conference on Systems and Control*, pp. 697–701, 2013. doi: 10.1109/ICoSC.2013.6750935.

[35] O. Aissa, S. Moulahoum, I. Colak, B. Babes and N. Kabache, "Analysis, design and real-time implementation of shunt active power filter for power quality improvement based on predictive direct power control," *in IEEE International Conference on Renewable Energy Research and Applications (ICRERA)*, pp. 79–84, 2016. doi: 10.1109/ICRERA.2016.7884400.

[36] H. A. Young, M. A. Perez, J. Rodriguez and H. Abu-Rub, "Assessing Finite-Control-Set Model Predictive Control: A Comparison with a Linear Current Controller in Two-Level Voltage Source Inverters," *IEEE Industrial Electronics Magazine*, vol. 8, no. 1, pp. 44–52, Mar. 2014. doi: 10.1109/MIE.2013.2294870.

[37] F. S. Guedes, N. Rocha, A. M. Maciel and A. J. Sguarezi Filho, "A Simple and Powerful Model Predictive Direct Power Control for DFIG," *in Brazilian Power Electronics Conference (COBEP)*, pp. 1–8, 2021. doi: 10.1109/COBEP53665.2021.9684128.

[38] M. Siami, D. A. Khaburi, A. Abbaszadeh and J. Rodríguez, "Robustness Improvement of Predictive Current Control Using Prediction Error Correction for Permanent-Magnet Synchronous Machines," *IEEE Transactions on Industrial Electronics*, vol. 63, no. 6, pp. 3458–3466, Jun. 2016. doi: 10.1109/TIE.2016.2521734.

## BIOGRAPHIES

**Felipe Suassuna Guedes,** was born in Patos, Paraíba, Brazil, in 1996. He received the B.S. degree in electrical engineering from the Federal Institute of Paraíba, Brazil, in 2019. Since 2020, he is working in M.S. degreeing electrical engineering in Federal University of Paraíba, João Pessoa, Brazil. His research interests include power electronics, electrical drives and renewable energy source.

**Nady Rocha,** was born in São Gabriel, Bahia, Brazil, in 1982. He received the B.S., M.S., and Ph.D. degrees in electrical engineering from the Federal University of Campina Grande, Campina Grande, Brazil, in 2006, 2008, and 2010, respectively. Since 2011, he has been with the Department of Electrical Engineering, Federal University of Paraíba, João Pessoa, where he is currently an Associate Professor of Electrical Engineering. His research interests include power electronics, renewable energy sources and electrical drives.

**Alvaro M. Maciel,** was born in Patos, Paraíba, Brazil, in 1982. He received the B.S., M.S., and Ph.D. degrees in electrical engineering from the Federal University of Campina Grande, Campina Grande, Brazil, in 2008, 2009, and 2015, respectively. Since 2015, he has been with the Course of Electrical Engineering (linked at Academic Unity 3), Federal Institute of Paraíba, João Pessoa, Brazil, where he is currently a Professor of electrical engineering. His research interests include power electronics, renewable energy sources, and electrical drives.

**Alfeu J. Sguarezi Filho,** received the master's and Ph.D. degrees from the University of Campinas, Campinas, Brazil, in 2007 and 2010, respectively. He is currently a Professor with the Federal University of ABC, Santo André, Brazil, teaching in the areas of electrical machines, power electronics, and electrical drives. His current research interests include machine drives, wind and photovoltaic energies, doubly fed induction generators, power control, and electrical power systems.